

# Numerical Simulation of Dynamic Elasto Visco-plastic Fracture Using Moving Finite Element Method

T. Fujimoto<sup>1</sup> and T. Nishioka<sup>1</sup>

**Abstract:** In the dynamic fracture of metallic material, some cracks propagate with the incidence of plastic deformation, and distinct plastic strain remains near the post-propagation area. In order to elucidate these dynamic nonlinear fracture processes, the moving finite element method is developed for nonlinear crack propagation. The  $T^*$  integral is used as the parameter to estimate crack tip condition. First, the effect of material viscosity and crack propagation velocity have been discussed based on the numerical results for fracture under pure mode I high speed loading. Under mixed mode loading, numerical simulations for fracture path prediction are demonstrated for various crack propagation velocities. In these numerical simulations, the maximum hoop stress criterion is used to predict the fracture path.

**keyword:** Nonlinear fracture,  $T^*$  integral, Moving finite element method, Wake zone, Non-straight crack propagation

## 1 Introduction

In many crush accidents, earthquakes and etc., permanent deformation have been caused in the structures. Traces of fast crack propagation can be observed in some cases of these accidents. The large deformation occurs near the crack tip domain and the ductile fracture condition dominates the near-field of crack tip. However, the crack propagation velocity reaches a few meters per second or more than it, the propagation velocity is too fast for ductile fracture mode to prevail. In these phenomena, distinct plastic deformation (wake zone) remains near the post-crack propagation area.

For the dynamic crack propagation with large deformation, the accuracy of conventional experimental measurements, such as image correlation method and etc. For example the image correlation method is not enough to estimate the fracture mechanics parameter. Therefore, nonlinear numerical analyses have been used to investigate

the crack propagation behavior [Fujimoto and Nishioka (2003, 2004)].

Some numerical techniques have been proposed to estimate the crack propagation phenomena. The nodal release technique [Kobayashi, Mall, Urabe and Emery (1978)] [Fujimoto, Akashi, and Nishioka (2000)] for finite element analyses is very popular as the numerical method to simulate fracture problems. However, because the fracture path have to be represented by element boundaries in the nodal release method, application of the nodal release method is difficult for the simulation to predict non-straight fracture path. Recently, various numerical techniques and modeling have been proposed, such as the cell method [Ferretti (2003)], the novel non-hypersingular time-domain traction boundary element method [Zhang and Savaidis (2003)], the symmetric Galerkin boundary element method [Han and Atluri (2002)] and the material point method [Nairn (2003)]. To simulate non-straight crack propagation and dynamic crack propagation, Nishioka [Nishioka (1994)] proposed the moving finite element method. In the moving finite element method, the boundary condition near the crack tip is accurately expressed by translation of fine mesh subdivision. The moving finite element method can be applied to simulate complex dynamic fracture problem, such as dynamic crack bifurcation [Nishioka, Furutuka, Tchouikov and Fujimoto (2002), Tchouikov, Nishioka and Fujimoto (2004)]. Because main targets of the conventional moving finite element method were dynamic elastic crack propagation phenomena and the strain near the post-propagation area were disappeared by unloading effect, measurement of deformation near the post-propagation area was not treated as important problem.

In this study, the moving finite element method is developed to simulate non-straight crack propagation with large deformation. Wake zone can be accurately simulated in the proposed moving finite element method, and the  $T^*$  integral values using extending near-field integral path are calculated to discuss the crack tip condition for

---

<sup>1</sup> Kobe University, Kobe, Japan

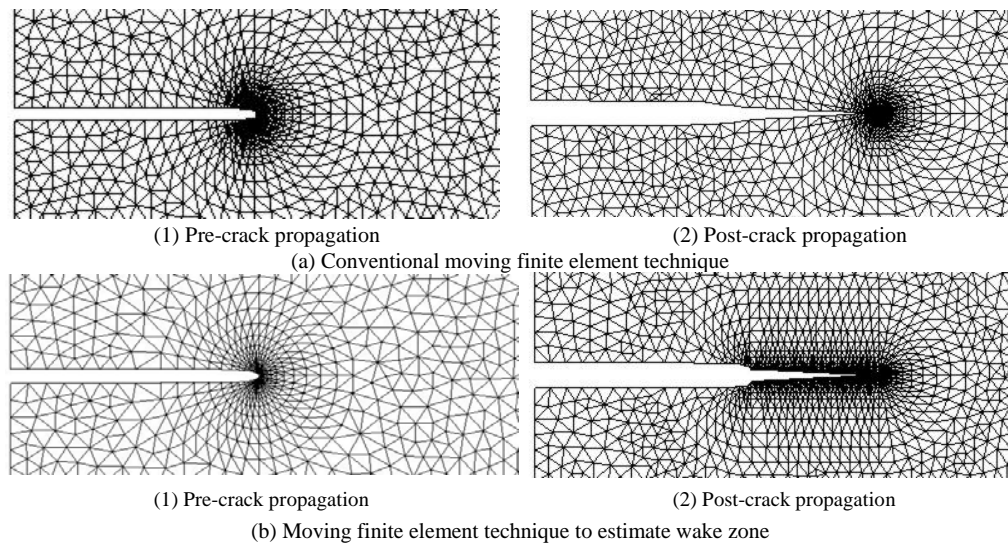


**Figure 1** : Fine mesh subdivision near propagating crack tip

dynamic elasto visco-plastic fracture. This developed moving finite element method is also applied to predict fracture path under mixed mode loading. In the path prediction mode simulations, the crack propagation velocity is systematically changed, and the dependence of crack propagation direction is discussed.

## 2 Moving finite element method

In the moving finite element method [Nishioka (1994)], since the fine mesh subdivision (moving elements) is moved with crack tip movement, accurate boundary condition near a propagating crack tip is expressed for non-straight and/or dynamic crack propagation, as shown in Fig. 1(a). The Delaunay automatic triangulation technique [Taniguchi (1992)] is used for the mesh regeneration around the moving elements in the moving finite element method using triangular elements [Nishioka, Tokudome and Kinoshita (2001)]. The moving elements achieve the precise calculation of stress and strain singular distributions in the near-field of crack tip. For nonlinear fracture based on the infinitesimal deformation theory, the modified variational principle has been proposed to formulate the nonlinear moving finite element method [Nishioka and Wang (1999)].

In some cases of nonlinear fracture with dynamic large deformation, distinct plastic deformation remains in post-crack propagation area. Accurate estimation of irreversible deformation energy is required to compute path integral parameter for the propagating crack tip. In

the conventional moving element technique, the plastic wakes have been numerically vanished by the parameter mapping and the coarse mesh allocation. In this study, fine mesh subdivision is allocated near the crack-propagation area to accurately estimate plastic strain distribution [Fujimoto and Nishioka (2004)], as shown in Fig. 1(b).

Here, fine nodal layers are created based on the fracture path. This procedure can be applied to non-straight fracture path. Based on these nodal layers, the fine mesh subdivision is automatically generated in whole post-propagation area.

After mesh translation, the numerical method requires the information for dynamic elasto visco-plastic deformation (displacements, velocities, accelerations, plastic strain, equivalent stress, yield surfaces and stress work densities) at newly created nodes and integration points. The field variables on the new mesh subdivision are obtained through the finite element interpolation from the parameters at old nodes or elements. Here, field variables at time step  $t_0$  on new mesh subdivision are expressed by superscript  $(t_0)$ . Solution at next time step  $t_0 + \Delta t$  on new mesh subdivision is calculated based on the mapped field variables  $(t_0)$ .

The variational principle has been derived to formulate the finite element equations based on the foregoing field variables  $(t_0)$  [Nishioka and Wang (1999)]. Because large deformation occurs in the material, the variational

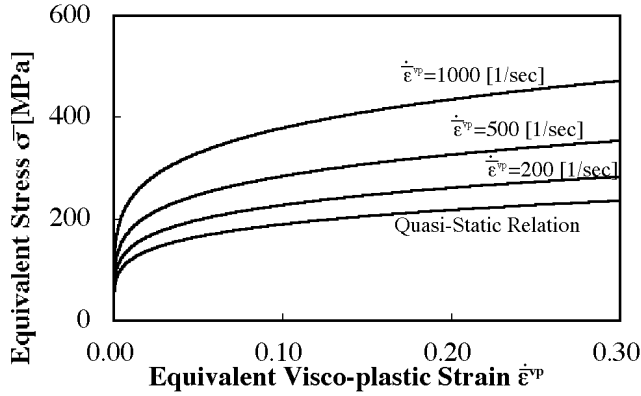


**Figure 2** : Equivalent stress-strain relation for the Malvern constitutive equation

**Table 1** : Material parameters

E	Young's modulus [GPa]	210
v	Poisson's ratio	0.3
D	Visco-plastic coefficient [1/s]	1000
F	Referential stress [MPa]	300
n	Strain hardening exponent	0.2
ρ	Mass density [kg/m <sup>3</sup> ]	7900

principle is formulated by rate-form:

$$\begin{aligned}
 & \int_V \dot{\pi}_{ij} \Delta t \delta \dot{u}_{i,j} dV + \int_V \rho \frac{\partial (\dot{u}_i^{t_0 + \Delta t})}{\partial t^2} \Delta t \delta \dot{u}_i dV \\
 &= \int_{S_r} (\bar{r}_i^{(t_0)} + \dot{r}_i \Delta t) \delta \dot{u}_i dS - \int_V \sigma_{ij}^{(t_0)} \delta \dot{u}_{i,j} dV \\
 & - \int_V \rho \dot{u}_i^{(t_0)} \delta \dot{u}_i dV, \quad (1)
 \end{aligned}$$

where,  $\sigma_{ij}$ ,  $\pi_{ij}$ ,  $u_i$  and  $\bar{r}_i$  denote components of the Cauchy stress, the Lagrange stress, displacement and traction force, respectively.  $\dot{(\ )}$  means the time derivative of  $(\ )$ . Displacement rate  $\dot{u}_i$  is independent variable in this equation. In the material, geometric boundary condition is changed by the crack propagation. Equation 1 satisfies the equilibrium condition and boundary condition at generic time step  $t_0 + \Delta t$ . The Newmark  $\beta$  method is used for the time integration of the finite element equations of motion. In this study, the Newmark's parameters are set to be  $\beta=1/4$  and  $\delta=1/2$  to satisfy the unconditionally sta-

ble condition [Bathe and Wilson (1976)].

The Malvern type constitutive equation [Malvern (1951)] is used to express visco-plastic response of material. The formula shows a visco-plastic strain rate based on the quasi-static flow stress. The constitutive equation is written as:

$$\dot{\bar{\epsilon}} = \frac{\bar{\sigma}}{E} + D \left( \frac{\bar{\sigma}}{\sigma_f} - 1 \right), \quad (2)$$

where  $\bar{\sigma}$ ,  $\bar{\epsilon}$ , E and D denote the equivalent stress, the equivalent strain, the Young's modulus and the visco-plastic coefficient, respectively.  $\sigma_f$  is the quasi-static flow stress, which is expressed by following equation:

$$\bar{\epsilon} = \frac{\sigma_f}{E} + \left( \frac{\sigma_f}{F} \right)^{\frac{1}{n}}, \quad (3)$$

where n and F denote the strain hardening exponent and the referential stress, respectively. The values of each parameter are shown in Tab. 1. For various equivalent visco-plastic strain rates, the relations between the equivalent stress and equivalent visco-plastic strain are shown in Fig. 2.

Here, the large deformation theory, which has been proposed by Tomita et.al. [Tomita, Shindou, Asada and Goto (1988)], is used to formulate the finite element equations for elasto visco-plastic deformation. Only outline is explained here. The formulation is based on the relation between the stress rate and the strain rate. Here, the J<sub>2</sub> deformation theory [Budiansky (1959)] is used to express the visco-plastic strain rate. In this theory, the effects of non-coaxiality of the deviatoric stress tensor  $\sigma'_{ij}$  and the visco-plastic strain rate tensor  $\dot{\epsilon}_{ij}^{vp}$  are considered. By using the deformation theory, the stress rate  $\dot{\sigma}_{ij}$  is obtained as:

$$\dot{\sigma}_{ij} = D_{ijkl}^e \left\{ \dot{\epsilon}_{kl} - \frac{3}{2} \frac{\dot{\bar{\epsilon}}^{vp}}{\bar{\sigma}} \sigma'_{kl} - \frac{3}{2} \omega \frac{\bar{\epsilon}^{vp}}{\bar{\sigma}} \left( \dot{\sigma}'_{kl} - \frac{\dot{\bar{\sigma}}}{\bar{\sigma}} \sigma'_{kl} \right) \right\}, \quad (4)$$

where,  $D_{ijkl}^e$ ,  $\dot{\epsilon}_{kl}$ ,  $\sigma'_{kl}$  and  $\bar{\sigma}$  denote the elastic stiffness tensor, the strain rate tensor, the deviatoric stress tensor and the equivalent stress, respectively.  $\omega$  is the parameter that shows the non-coaxiality of the deviatoric stress tensor and the visco-plastic strain rate tensor. In this study,  $\omega=1$  is used to assume that the coaxiality between the deviatoric stress tensor and the visco-plastic strain rate tensor is perfectly preserved.

Here, the stress rate  $\dot{\sigma}_{ij}$  and the strain rate  $\dot{\epsilon}_{kl}$  are replaced with the Jaumann rate of the Kirchhoff stress  $S_{ij}$  and the deformation rate  $d_{kl}$ , respectively [Tomita, Shin-dou, Asada and Goto (1988)]. In this reference, to improve the stability of calculation for nonlinear deformation, following constitutive equation has been introduced by using the tangent modulus method:

$$S_{ij} = (L'_{ijkl}{}^{\text{tan}} - F_{ijkl}) d_{kl} - \frac{\dot{\bar{\epsilon}}_n^{vp}}{1 + \xi} D_{ijkl}^e \frac{3\sigma'_{kl}}{2\bar{\sigma}}, \quad (5)$$

where,  $\dot{\bar{\epsilon}}_n^{vp}$  means the equivalent visco-plastic strain rate at current time step. Each term for the Malvern type equation are expressed by:

$$L'_{ijkl}{}^{\text{tan}} = \frac{1}{\bar{\sigma}/\bar{\epsilon}^{vp} + 3G} \left[ \frac{\bar{\sigma}}{\bar{\epsilon}^{vp}} D_{ijkl}^e + 3G \left( \frac{1}{3} \delta_{ij} \delta_{kl} \frac{2G(1+\nu)}{1-2\nu} + \frac{3G\sigma'_{ij}\sigma'_{kl}}{\bar{\sigma}^2} \right) \right] - \frac{1}{h} \frac{\xi}{1+\xi} \frac{9\sigma'_{ij}\sigma'_{kl}}{4(\bar{\sigma})^2}, \quad (6)$$

$$\begin{aligned} \xi &= \Delta t \cdot \left( D_{ijkl}^e \frac{9\sigma'_{kl}\sigma'_{kl}}{4(\bar{\sigma})^2} - \frac{\partial \bar{\sigma}}{\partial \bar{\epsilon}^{vp}} \right) \frac{\partial \dot{\bar{\epsilon}}^{vp}}{\partial \bar{\sigma}} \\ &= \Delta t \cdot \left\{ D_{ijkl}^e \frac{9\sigma'_{kl}\sigma'_{kl}}{4(\bar{\sigma})^2} - \left( \frac{1}{D} \dot{\bar{\epsilon}}^{vp} + 1 \right) nF(\bar{\epsilon}^{vp})^{n-1} \right\} \frac{D}{\sigma_f}, \end{aligned} \quad (7)$$

$$F_{ijkl} = \frac{1}{2} (\sigma_{lj}\delta_{ki} + \sigma_{kj}\delta_{li} + \sigma_{li}\delta_{kj} + \sigma_{ki}\delta_{lj}), \quad (8)$$

where, G denotes the shearing modulus.

### 3 T\* integral

The T\* integral [Atluri, Nishioka and Nakagaki (1984)] has excellent far-field path independence for any material constitutive relation under quasi-static as well as dynamic conditions. The T\* integral is defined for the dynamic nonlinear fracture in an elastic plastic material under arbitrary loading history. In some literatures [Nishioka, Kobashi and Atluri (1988)][Nishioka Yagami (1988)], the T\* integral has been applied to dynamic nonlinear fracture problems. And, it have been demonstrated that the T\* integral can be used as valid fracture mechanics parameter.

The T\* integral is evaluated by following integration:

$$\begin{aligned} T_k^* &= \int_{\Gamma_\epsilon} [(W + K) n_k - t_i u_{i,k}] dS \\ &= \int_{\Gamma + \Gamma_c} [(W + K) n_k - t_i u_{i,k}] dS \\ &\quad + \int_{V_{\Gamma-V_c}} [\rho \dot{u}_i u_{i,k} - \rho \dot{u}_i \dot{u}_{i,k} + \sigma_{ij} u_{i,jk} - W_{,k}] dS, \end{aligned} \quad (9)$$

where, W and K mean the stress working density and the kinetic energy density, respectively.  $n_k$ ,  $t_i$  and  $\rho$  are the components of unit outward normal vector on the integral path, the traction and the mass density, respectively.  $\Gamma_\epsilon$ ,  $\Gamma$  and  $\Gamma_c$  denote a near-field path, far-field path and crack surface path, respectively. Each integral path setting in a nonlinear deformation solid is shown in Fig. 3. The T\* integral was originally defined on the near field integral path  $\Gamma_\epsilon$ , which surrounds crack tip. The far-field measurement form of the T\* integral can be derived using the divergence theory.

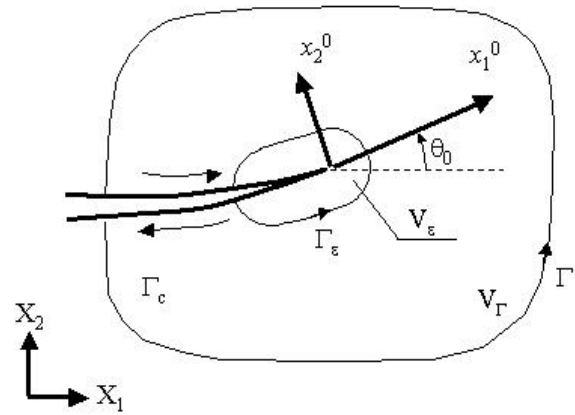
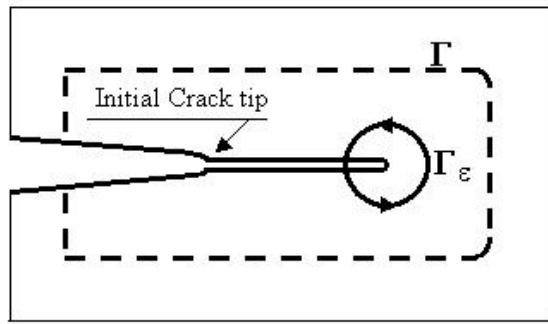


Figure 3 : Definition of integral paths

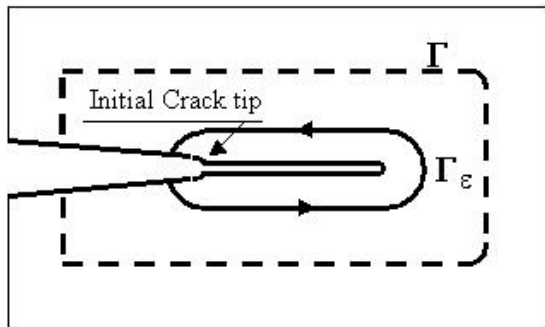
The T\* integral is equivalent to the energy flow rate to the near-field domain  $V_\epsilon$ . For the non-straight crack propagation, the crack-axis components of the T\* integral,  $T_i^{*0}$  can be evaluated by the coordinate transformation, as shown by the following formula:

$$T_\ell^{*0} = \alpha_{\ell k}(\theta_0) T_k^*, \quad (10)$$

where  $\alpha_{\ell k}$  is the coordinate transformation tensor and  $\theta_0$  is the angle between the global axis  $X_1$  and the crack axis  $x_1^0$ .



(a) Moving near-field path



(b) Extending near-field path

**Figure 4 :** Integral path models of  $T^*$  for crack propagation problem

In general case of nonlinear fracture, the  $T^*$  values depend on the size and the shape of the near-field integral path  $\Gamma_\epsilon$ . Therefore, some researchers proposed some types of near-field integral path [Nishioka, Fujimoto and Atluri (1989)][Okada and Atluri (1999)]. Figure 4 shows the near-field integral paths to estimate the  $T^*$  integral for propagating crack tip. In this figure,  $\Gamma$  means constant far-field integral path.

In steady state crack propagation, the  $T^*$  value, which is integrated using the moving near field path, is too small compared with the  $T^*_{IC}$  (crack initiation criterion). On the other hand, the  $T^*$  value based on the extending near-field path remains in the same order of the  $T^*_{IC}$ . Okada reported that the  $T^*$  values depend on the amount of deformation energy in near-field domain  $\Gamma_\epsilon$  [Okada and Atluri (1999)]. For the nonlinear fracture with large deformation, permanent deformation remains inside near-field path. In the case using the extending near-field path, the effect of plastic deformation have to be accurately estimated on overall integral domain.

In this study, wake zone is accurately simulated by the

developed moving element technique, as shown in the foregoing section. The extending near field path is defined based on the fracture path, and it is independent on the mesh subdivision.

In the authors' group, the local symmetry criterion [Goldstein and Salganik (1974)] and maximum hoop stress criterion [Erdogan and Sih (1963)] have been mainly used for numerical prediction of fracture path. For nonlinear crack propagation, the local symmetry near the crack tip can be evaluated based on the  $T^*_2$  value. If the local symmetry criterion is applied in the moving finite element method,  $T^*_2 = 0$  condition have to be always satisfied during crack propagation. In this case, iterative operations are required in each time step calculation [Nishioka, Tokudome, and Kinoshita (2001)].

#### 4 Crack propagation under mode I loading

##### 4.1 Numerical model

In initial mesh subdivision,  
 Total elements : 3788  
 Total nodes : 2000  
 Global strain rate :  $\dot{u}_2 / W = 100 [1/s]$   
 Time step increment :  $2.0 \mu s$   
 Crack propagation velocity  $C$  :  
 $C/C_s = 0.01, 0.02, 0.05$   
 where shear wave velocity  
 $C_s = 3198 \text{ m/sec}$

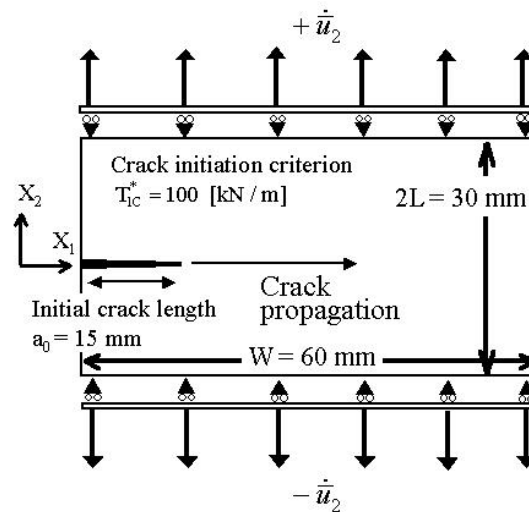


**Figure 5 :** Numerical specimen for straight crack propagation under mode I loading

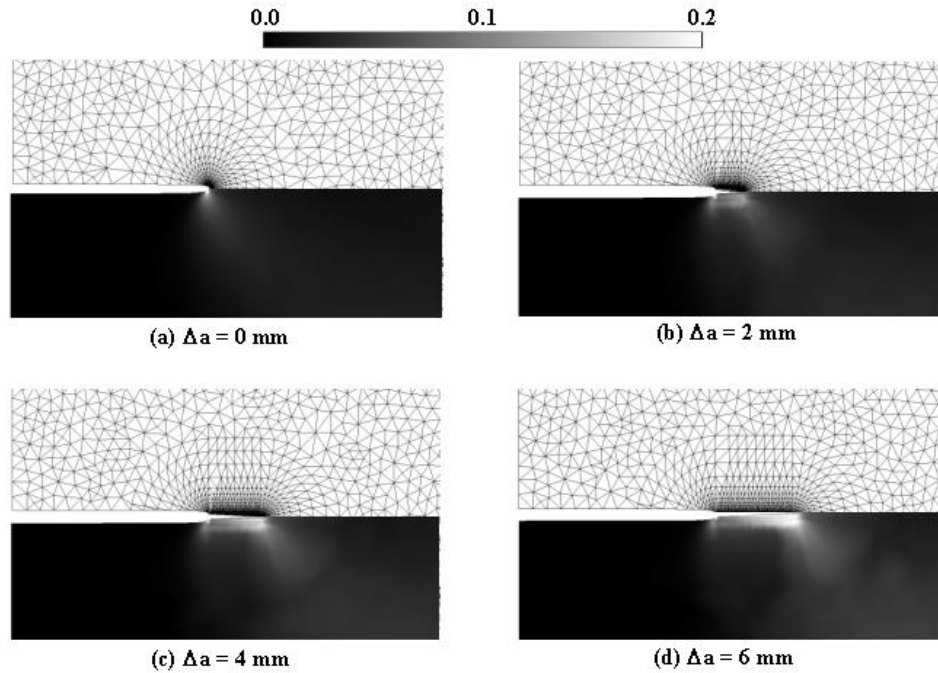


Figure 6 : Mesh subdivisions and equivalent visco-plastic strain distributions for straight crack propagation  $C/C_s = 0.01$

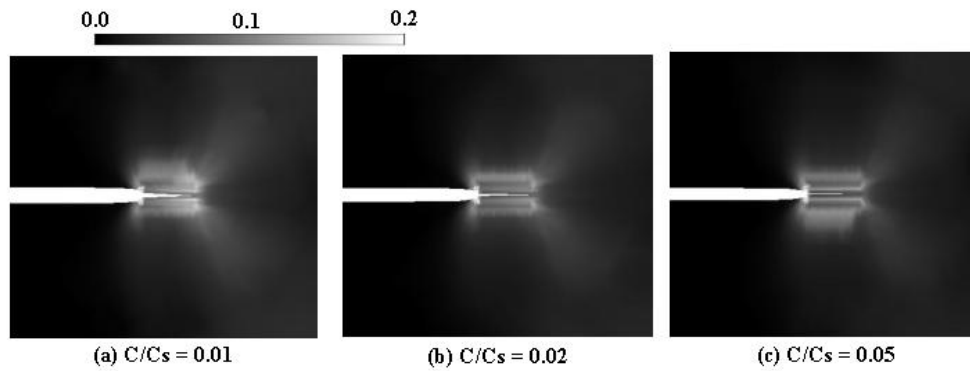


Figure 7 : Visco-plastic strain distributions for each crack propagation velocity

In this section, elasto visco-plastic deformations are treated with straight crack propagation under pure mode I loading. Figure 5 shows the numerical conditions and the shape of specimen. Mode I loading is caused by the constrained displacement rate  $\dot{u}_2$  at the upper and lower ends of the specimen. The plane stress condition is assumed in these deformations. When the  $T^*_1$  value reaches  $100\text{kN/m}$  ( which is assumed as the initial fracture toughness  $T^*_{1C}$ ), crack propagation starts in the numerical model. To discuss the dependence of fracture behavior, the crack propagation velocity  $C$  is systematically

changed as:

$$C/C_s = 0.01, 0.02, 0.05. \tag{11}$$

where,  $C_s$  means the shear wave velocity. In each numerical analysis, the fracture with constant crack propagation velocity is assumed.

#### 4.2 Numerical results and discussions

Figure 6 shows the mesh subdivisions and the equivalent visco-plastic strain distributions in the case of  $C/C_s$

= 0.01. The distinct plastic deformations have been simulated by the fine mesh subdivision near post-propagation area. The residual plastic deformations are not vanished by the mesh translation and the parameter mapping of the moving finite element method.

Figure 7 shows the equivalent visco-plastic strain distributions for each crack propagation velocity. The enlargement of distinct plastic zone does not depend on the crack propagation velocity. On the other hand, the difference of strain intensity can be observed in Fig. 7. In the faster crack propagation problem  $C/C_s = 0.05$ , strain rate at the vicinity of crack tip increases and therefore the strain gradients become larger than the case of the slower crack propagation velocity.

Here, the extending near-field path model is applied to estimate the  $T^*$  integral value. The length between the front of near-field path and crack tip is 0.5mm. The near-field domain includes the 4 layers of fine elements. The shape of near-field path  $\Gamma_\epsilon$  has to be changed along the crack propagation path. The shape of  $\Gamma_\epsilon$  is monitored in the numerical program. One of the monitored results is shown in Fig. 8. The integral path  $\Gamma_\epsilon$  is perfectly closed, and accurate  $T^*$  value can be calculated by the numerical integration. Five far-field integral paths have been prepared to evaluate the  $T^*$  integral. The  $T^*$  values for each far-field path are shown in Fig. 9. Excellent path independence of the  $T^*$  can be confirmed and the path independence is maintained during fast crack propagation.

The  $T^*$  integral histories during crack propagation are shown in Fig. 10. The  $T^*$  values range from 30 to 250 kN/m, and their orders are not small compared with the initial fracture toughness  $T^*_{1C}$ . These  $T^*$  values from the extending near-field path includes the effects of wake zone. For the moving near-field path model to estimate the  $T^*$ , many researchers [Okada and Atluri (1999)][Fujimoto and Nishioka (2001)] reported that  $T^*$  values rapidly decreased after the crack initiation.

The crack propagation velocity affects the  $T^*$  values considerably. In the case of faster crack propagation, the material viscosity increases the deformation resistance in near-field domain  $V_\epsilon$ . This trend can be also observed in stress and strain distributions near the crack tip (see Fig.7). By the increase of the stress work density in the near-field of the faster crack propagation, the  $T^*$  integral values increase.

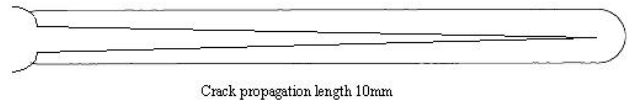


Figure 8 : Extending near-field integral path in numerical simulation

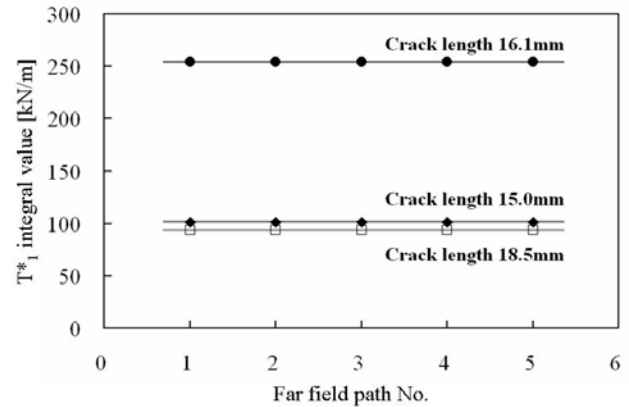


Figure 9 : Far field path independence of  $T^*$  integral for  $C/C_s = 0.01$

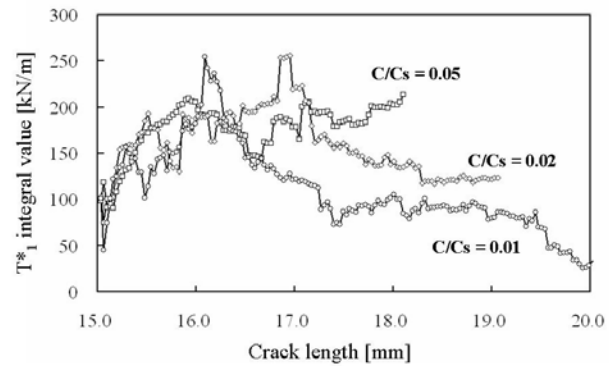


Figure 10 : Histories of  $T^*$  integral values for straight crack propagations

## 5 Crack propagation under mixed mode loading

### 5.1 Numerical model

Under mixed mode loading, the moving finite element method has been applied to predict dynamic nonlinear crack propagation path. The plane stress condition is also assumed in this section. The shape of the specimen under mixed mode loading is shown in Fig. 11. The crack initiation is assumed to occur at  $T^*_{1C} = 100$  kN/m. To cause mixed mode fracture condition, constrained dis-

In initial mesh subdivision,  
 Total elements : 5002      Total nodes : 2600  
 Loading angle  $\phi = 45$  deg.  
 Global strain rate :  $\dot{\bar{u}}_x / W = 100$  [1/s]  
 Time step increment :  $2.0\mu\text{s}$   
 Crack propagation velocity  $C$  :  
 $C/C_s = 0.01, 0.02, 0.03$ , where  $C_s = 3198$  m/sec

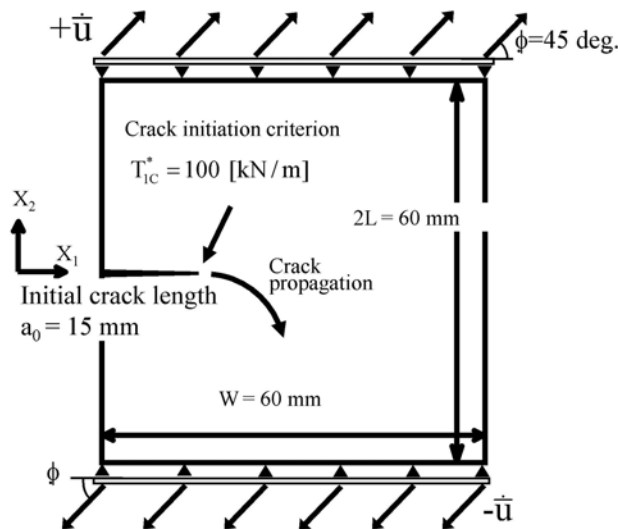


**Figure 11** : Numerical specimen to predict crack propagation path under mixed mode loading

placements are imposed on the edges of the specimen. The constrained displacement angle  $\phi$  is 45 degrees. In these numerical simulations, the crack propagation direction is numerically predicted using the maximum hoop stress criterion [Erdogan and Sih (1963)]. In each time step, the hoop stress distribution has been evaluated on the circular line  $\Gamma_n$ . The length between  $\Gamma_n$  and the current crack tip is 0.24mm. Constant crack propagation velocity is assumed, and numerical simulations have been performed for:

$$C/C_s = 0.01, 0.02, 0.03 \quad (12)$$

### 5.2 Numerical results and discussions

Figure 12 shows the mesh subdivisions and the equivalent visco-plastic strain distributions for each crack propagation velocity. Details of non-straight fracture paths have been expressed by the fine mesh subdivision near the post-propagation area. By these fine mesh subdivi-

sions, the residual plastic strain distributions near the crack propagation area is accurately simulated, as shown in Fig. 12 (b). Crack propagation angle depends on the crack propagation velocity. Faster crack propagation rate restrains the fracture path from curving. In Fig. 12, the local symmetries near the propagating crack tip can be observed from these distributions, though the maximum hoop stress criterion is used as fracture path prediction theory. At the early stage of crack propagation, unsteady fracture condition occurs by the crack kinking and dynamic crack initiation. Therefore, the plastic strain intensities near the initial crack tip are rapidly changed by the crack initiation.

Based on these numerical deformation fields, the  $T^*$  values for the propagating crack tip have been integrated. The far-field path independence of the  $T^*$  integral is also kept in the non-straight crack propagation, as shown in Fig. 13. The variations of the  $T_1^{*0}$  values are shown in Fig. 14. In these numerical analyses, the dependence of the  $T^*$  integrals on crack propagation velocity can not be observed, because the propagating crack tip condition do not reaches steady state. After the crack initiation,  $T_1^{*0}$  have been decreased and negative  $T_1^{*0}$  values have been calculated though crack does not close. In order to clarify the crack initiation behavior under mixed loading, further investigation will be required for the criterion of crack initiation, the appropriate size of  $\Gamma_e$  to estimate the  $T^*$ , the fracture path prediction theory for dynamic elasto visco-plastic fracture and etc.

## 6 Conclusion

In this study, the moving finite element method has been developed for crack propagation with distinct permanent strain near post-propagation area. The proposed numerical simulation correctly works to simulate not only straight crack propagation phenomena but also non-straight propagation phenomena. Based on the numerical deformation fields, the  $T^*$  integrals have been calculated using the extending near-filed integral path. For the straight crack propagation, the dependence of the  $T^*$  integral on crack propagation velocity has been observed. For the numerical fracture path prediction under mixed mode loading fracture, the  $T^*$  integration has kept the far-field path independence. The  $T^*$  values and fracture path depend on the crack propagation velocity.

**Acknowledgement:** This work is supported by the

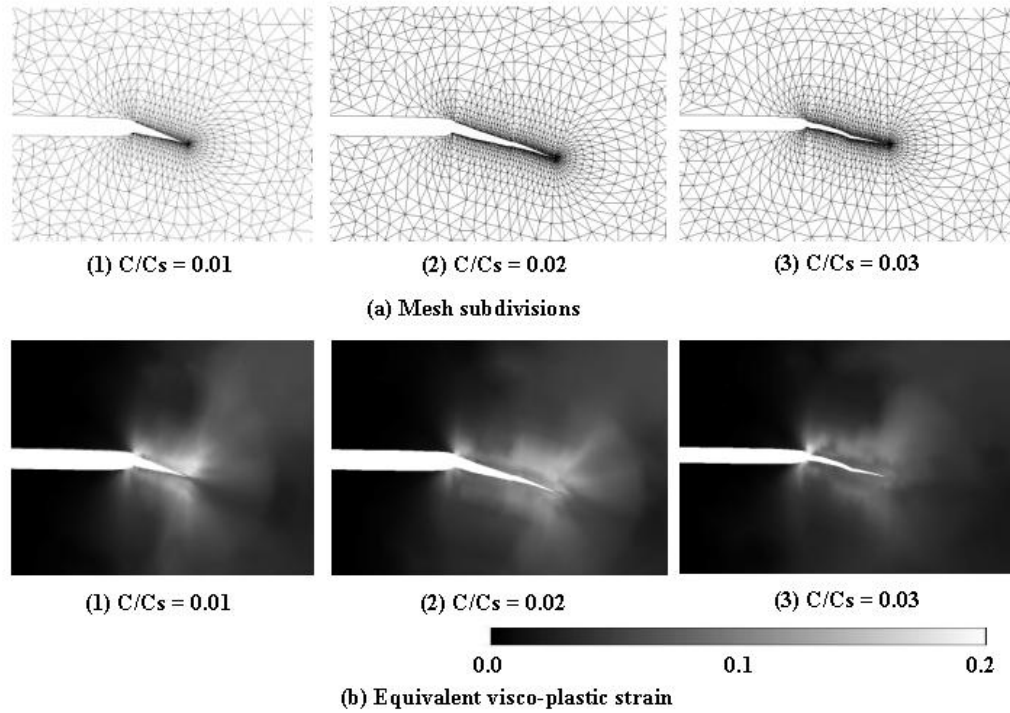


Figure 12 : Mesh subdivisions and visco-plastic strain distributions under mixed mode loading

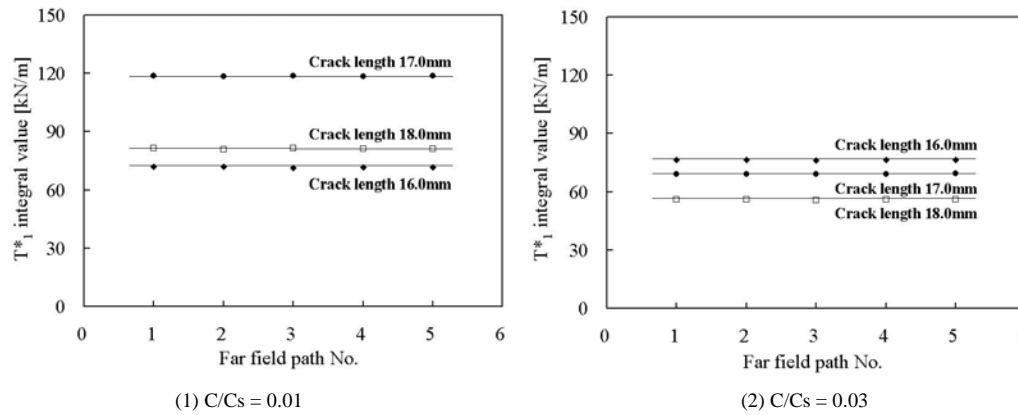


Figure 13 : Far field path independence of  $T^*$  integral for non-straight crack propagations

Grant-in-Aid for Scientific Research from the Ministry of Education in Japan (No.16760074 and No.14205019).

References

Atluri, S.N.; Nishioka, T.; Nakagaki, M. (1984): Incremental Path-Independent Integrals in Inelastic and Dynamic Fracture Mechanics. *Eng. Fract. Mech.*, 20, 2, pp.209-244.

Bathe, K. J.; Wilson, E. L. (1976): *Numerical Methods*

*in Finite Element Analysis*. Prentice-Hall, New Jersey.

Budiansky, B. (1959): A Reassessment of Deformation Theories of Plasticity. *Trans. ASME. J. Appl. Mech.*, vol.26, pp.259.

Erdogan, F.; Sih, G.C. (1963): On The Crack Extension in Plates under Plane Loading and Transverse Shear. *Basic Eng.*, ASME, 85, pp.519-527.

Ferretti, E. (2003): Crack Propagation Modeling by Remeshing Using the Cell Method (CM). *CMES: Com-*

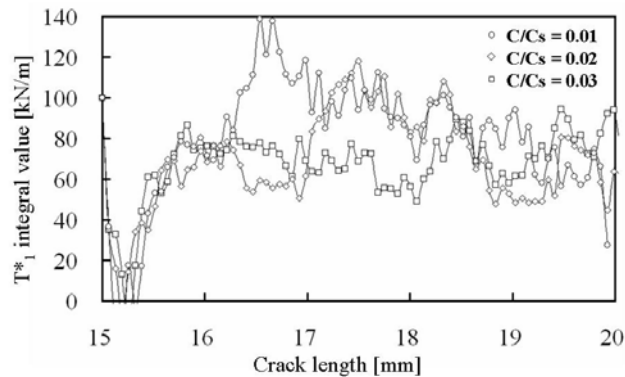


**Figure 14** : Histories of  $T^*$  integral values for non-straight crack propagations

*puter Modeling in Engineering & Sciences*, vol.4, no.1, pp.51-72.

**Fujimoto T.; Akashi T.; Nishioka T.** (2000): Crack-tip Deformation Behavior under Nonlinear and Dynamic Large Deformation of Metallic Materials. *Advances on Computational Engineering and Sciences*, (S.N. Atluri and F.W. Brust, editors), II, Tech Science Press, Palm-dale, CA, USA, pp.1860-1865.

**Fujimoto, T.; Nishioka, T.** (2001): Numerical Analysis of Fracture under Dynamic Large Deformation Using a Moving Finite Element Method. *Advances in Computational Engineering and Sciences*, (S.N. Atluri, T. Nishioka and M. Kikuchi, Editors), Tech Science Press, Chapter 7, Paper 21, pp.1-6.

**Fujimoto, T.; Nishioka, T.** (2003): Fracture Path Predictions using Numerical Simulations for Dynamic Thermo Elasto Visco Plastic Fracture. *Advances on Computational and Experimental Engineering and Sciences*, Chapter 11, No.433, Tech Science Press, 6pages.

**Fujimoto T.; Nishioka T.** (2004): Numerical Simulation of Dynamic Elasto Visco-plastic Crack Propagation with Wake Zone. *Advances on Computational and Experimental Engineering and Sciences*, Tech Science Press, pp.1821-1826.

**Goldstein R.V.; Salganik R. L.** (1974): Brittle Fracture of Solids with Arbitrary Cracks. *International Journal of fracture*, vol.10, pp.507-523.

**Han, Z. D.; Atluri, S. N.** (2002): SGBEM (for Cracked Local Subdomain) – FEM ( for Uncracked Global Structure) Alternating Method for Analyzing 3D Sur-

face Cracks and Their Fatigue-Growth. *CMES: Computer Modeling in Engineering & Sciences*, vol.3, no.6, pp.699-716.

**Kobayashi A.S.; Mall S.; Urabe Y.; Emery A.F.** (1978): Fracture Dynamic Analysis of Crack Arrest Test Specimen, *Numerical Methods in Fracture Mechanics*, Univ. College, Swansea, pp.709-720.

**Malvern, L.E.** (1951): The Propagation of Longitudinal Waves of Plastic Deformation in a Bar of Material Exhibiting a Strain-Rate Effect, *ASME J. Appl. Mech.*, vol.18, pp.203-208.

**Nairn, J.A.** (2003): Material Point Method Calculations with Explicit Cracks. *CMES: Computer Modeling in Engineering & Sciences*, vol.4, no.6, pp.649-664.

**Nishioka T.; Kobashi M.; Atluri S.N.** (1988): Computational Studies on Path Independent Integrals for Non-Linear Dynamic Crack Problems, *Computational Mechanics*, 3, pp.331-342.

**Nishioka T.; Yagami H.** (1988): Invariance of the Path Independent  $T^*$  integral in Nonlinear Dynamic Fracture Mechanics, with Respect to the Shape of a Finite Process Zone, *Engineering Fracture Mechanics*, 31, 3, pp.481-491.

**Nishioka T.; Fujimoto, T.; Atluri, S.N.** (1989): On the Path Independent  $T^*$  Integral in Nonlinear and Dynamic Fracture Mechanics, *Nuclear Engineering and Design* No.111, pp.109-121.

**Nishioka, T.** (1994): The State of the Art in Computational Dynamic Fracture Mechanics, *JSME International Journal*, Series A, vol.37, No.4, pp.313-333.

**Nishioka, T.; Wang, Z.M.** (1999): The  $T^*$  Integral and the Separated  $T^*$  Integrals for Elastic-Plastic Interfacial Cracks, *Constitutive and Damage Modeling of Inelastic Deformation and Phase Transformation*, (A.S. Khan, editor), Neat Press, Fulton, Maryland, pp.741-744

**Nishioka, T.; Tokudome, H.; Kinoshita M.** (2001): Dynamic Fracture-Path Prediction in Impact Fracture Phenomena Using Moving Finite Element Method Based on Delaunay Automatic Mesh Generation, *International Journal of Solids and Structures*, 38, No.30-31, pp.5273-5301.

**Nishioka, T.; Furutuka, J.; Tchouikov, S.; Fujimoto, T.** (2002): Generation-phase Simulation of Dynamic Crack Bifurcation Phenomenon using Moving Finite Element Method Based on Delaunay Automatic Triangula-

tion. *CMES: Computer Modeling in Engineering & Sciences*, vol.3, no.1, pp.129-145.

**Okada, H.; Atluri, S.N.** (1999): Further studies on the characteristics of the  $T^*\epsilon$  integral: Plane stress stable crack propagation in ductile materials, *Computational Mechanics*, 23, pp.339-352.

**Taniguchi, T.** (1992): *Automatic Mesh Generation for FEM: Use of Delaunay Triangulation*, Morikita Publ., (Japanese).

**Tchouikov, S.; Nishioka, T.; Fujimoto, T.** (2004): Numerical Prediction of Dynamically Propagating and Branching Cracks Using Moving Finite Element Method. *CMC: Computers, Materials & Continua*, vol.1, no.2, pp.191-204.

**Tomita, Y.; Shindou, A.; Asada, S.; Goto, H.** (1988): Deformation Behavior of a Strain Rate Sensitive Block under Plane Strain Tension, *Trans. JSME*, vol.54, Ser.A, pp.1124-1130.

**Zhang, Ch.; Savaidis, A.** (2003): 3-D Transient Dynamic Crack Analysis by a Novel Time-Domain BEM. *CMES: Computer Modeling in Engineering & Sciences*, vol.4, no.5, pp.603-612.

